Measurement of $\pi^0\pi^0$ production in two-photon collisions

H. Marsiske,[e,l] D. Antreasyan,[i] H. W. Bartels,[e] D. Besset,[k] Ch. Bieler,[h] J. K. Bienlein,[e] A. Bizzeti,[g] E. D. Bloom,[l] I. Brock,[c] K. Brockmüller,[e] R. Cabenda,[k] A. Cartacci,[g] M. Cavalli-Sforza,[b] R. Clare,[l] A. Compagnucci,[g] G. Conforto,[g] S. Cooper,[l] R. Cowan,[k] D. Coyne,[b] A. Engler,[c] K. Fairfield,[l] G. Folger,[f] A. Fridman,[l,*] D. Gaiser,[l] D. Gelphman,[l] G. Glaser,[f] G. Godfrey,[l] K. Graaf,[h] F. H. Heimlich,[h,g] F. H. Heinsius,[h] R. Hofstadter,[l] J. Irion,[i] Z. Jakubowski,[d] H. Janssen,[j] K. Karch,[m,e] S. Keh,[m] T. Kiel,[h] H. Kilian,[m] I. Kirkbride,[l] T. Kloiber,[e] M. Kobel,[f] W. Koch,[e] A. C. König,[j] K. Königsmann,[m] R. W. Kraemer,[c] S. Krüger,[h] G. Landi,[g] R. Lee,[l] S. Leffler,[l] R. Lekebusch,[h] A. M. Litke,[l] W. S. Lockman,[l] S. Lowe,[l] B. Lurz,[f] D. Marlow,[c] W. Maschmann,[h] P. McBride,[i] F. Messing,[c] W. J. Metzger,[j] H. Meyer,[e] B. Monteleoni,[g] B. Muryn,[d,†] R. Nernst,[h] B. Niczyporuk,[l] G. Nowak,[d] C. Peck,[a] P. G. Pelfer,[g] B.Pollock,[l] F. C. Porter,[a] D. Prindle,[c] P. Ratoff,[a] M. Reidenbach,[j] B. Renger,[c] C. Rippich,[c] M. Scheer,[m] P. Schmitt,[m] J. Schotanus,[j] J. Schütte,[f] A. Schwarz,[l] D. Sievers,[h] T. Skwarnicki,[e] V. Stock,[h] K. Strauch,[i] U. Strohbusch,[h] J. Tompkins,[l] H. J. Trost,[e] B. van Uitert,[l] R. T. Van de Walle,[j] H. Vogel,[c] A. Voigt,[e] U. Volland,[f] K. Wachs,[e] K. Wacker,[l] W. Walk,[j] H. Wegener,[f] D. A. Williams,[i,b] and P. Zschorsch[e]

(The Crystal Ball Collaboration)

[a]*California Institute of Technology, Pasadena, California 91125*
[b]*University of California at Santa Cruz, Santa Cruz, California 95064*
[c]*Carnegie-Mellon University, Pittsburgh, Pennsylvania 15213*
[d]*Cracow Institute of Nuclear Physics, PL-30055 Cracow, Poland*
[e]*Deutsches Elektronen Synchrotron DESY, D-2000 Hamburg, Germany*
[f]*Universität Erlangen-Nürnberg, D-8520 Erlangen, Germany*
[g]*INFN and University of Firenze, I-50100 Firenze, Italy*
[h]*Universität Hamburg, I. Institut für Experimentalphysik, D-2000 Hamburg, Germany*
[i]*Harvard University, Cambridge, Massachusetts 02138*
[j]*University of Nijmegen and NIKHEF, NL-6525 ED Nijmegen, The Netherlands*
[k]*Princeton University, Princeton, New Jersey 08544*
[l]*Stanford University, Department of Physics and High Energy Physics Laboratory, Stanford, California 94305 and Stanford Linear Accelerator Center, Stanford University, Stanford, California 94305*
[m]*Universität Würzburg, D-8700 Würzburg, Germany*

(Received 9 February 1990)

The reaction $e^+e^-\to e^+e^-\pi^0\pi^0$ has been analyzed using 97 pb^{-1} of data taken with the Crystal Ball detector at the DESY e^-e^+ storage ring DORIS II at beam energies around 5.3 GeV. For the first time we have measured the cross section for $\gamma\gamma\to\pi^0\pi^0$ for $\pi^0\pi^0$ invariant masses ranging from threshold to about 2 GeV. We measure an approximately flat cross section of about 10 nb for $W=m_{\pi^0\pi^0}<0.8$ GeV, which is below 0.6 GeV, in good agreement with a theoretical prediction based on an unitarized Born-term model. At higher invariant masses we observe formation of the $f_2(1270)$ resonance and a hint of the $f_0(975)$. We deduce the following two-photon widths: $\Gamma_{\gamma\gamma}(f_2(1270))=3.19\pm0.16\pm^{0.29}_{0.28}$ keV and $\Gamma_{\gamma\gamma}(f_0(975))<0.53$ keV at 90% C.L. The decay-angular distributions show the $\pi^0\pi^0$ system to be dominantly spin 0 for $W<0.7$ GeV and spin 2, helicity 2 in the $f_2(1270)$ region, with helicity 0 contributing at most 22% (90% C.L.).

INTRODUCTION

The production of states with even charge conjugation can be studied in two-photon collisions as they occur at e^+e^- storage rings. Measuring the two-photon couplings of mesons provides information on their charged constituents and thus helps in classifying states with respect to their $q\bar{q}$ content. That is why two-photon physics plays an important role in the search for four-quark and gluonic states—one of the key issues in hadron spectroscopy.

In the search for such states, the reaction $\gamma\gamma\to\pi\pi$ is of particular interest since $\pi\pi$ is a likely decay channel for many resonances in the mass region below 2 GeV. A variety of measurements of $\gamma\gamma\to\pi^+\pi^-$ already exists, showing three $\pi^+\pi^-$ invariant-mass regions with different physical features: Below 1 GeV a large $\pi^+\pi^-$ continuum and possibly the excitation of a broad scalar

resonance are observed. Between 0.9 and 1.5 GeV the cross section is dominated by the $f_2(1270)$ resonance. Scalar resonances such as $f_0(975)$ and $f_0(1300)$ are also expected to contribute in this region. At higher masses, again, a $\pi^+\pi^-$ continuum is present. Whereas all experiments agree quite well in the $f_2(1270)$ region and above, they show considerable differences in the low-mass regime.

(a) DM1/2 data ($0.3 \leq m_{\pi^+\pi^-} < 0.9$ GeV) show an excess over the Born-term expectation that is attributed to the formation of a broad scalar resonance $f_0(700)$ with a two-photon width of (10 ± 6) keV (Ref. 1).

(b) PLUTO data ($0.38 \leq m_{\pi^+\pi^-} < 1.7$ GeV) fall below the Born term at $\pi^+\pi^-$ masses around 0.6 GeV, but are fairly well described elsewhere by a coherent sum of Born-term and $f_2(1270)$ amplitudes.[2]

(c) DELCO and TPC/2γ data (~ 0.5 GeV $\leq m_{\pi^+\pi^-} < 2.0$ GeV) are fairly well described over the whole mass range by the same ansatz that PLUTO used.[3,4]

In the low-mass region, experiments face the problem of separating $\gamma\gamma \to \pi^+\pi^-$ from the kinematically similar electromagnetic processes $\gamma\gamma \to e^+e^-$ and $\gamma\gamma \to \mu^+\mu^-$. In this region, contrary to the $f_2(1270)$ region and above, these signals are large, compared to the $\pi^+\pi^-$ signal, and are difficult to subtract reliably. The analysis of the reaction $\gamma\gamma \to \pi^0\pi^0$ presented here does not suffer from those backgrounds. Furthermore, the $\gamma\gamma \to \pi^0\pi^0$ continuum is expected to be much smaller than $\gamma\gamma \to \pi^+\pi^-$ at low-invariant masses, so a resonance would be more apparent in the $\pi^0\pi^0$ channel.

The Born-term approximation for $\gamma\gamma \to \pi^+\pi^-$ (see, for example, Ref. 5) treats the pions as pointlike particles that do not interact strongly, with the photons directly coupling to their charge. Hence the Born term does not contribute directly to $\gamma\gamma \to \pi^0\pi^0$. Extensions to this simple model have been developed that embody the constraints of unitarity and analyticity together with the measured $\pi\pi$ and $K\bar{K}$ phase shifts, while respecting the QED low-energy theorem imposed by gauge invariance; see Refs. 6–8, and references therein.

Following Ref. 8, the amplitude $\mathcal{A}$ for $\gamma\gamma \to \pi^+\pi^-$ can be written as

$$\mathcal{A} = \mathcal{B} + \mathcal{C} + \mathcal{D} , \tag{1}$$

where $\mathcal{B}$ denotes the Born-term amplitude (i.e., π exchange in the t channel), $\mathcal{C}$ denotes exchanges other than π (e.g., ρ or ω exchange), and $\mathcal{D}$ is generated by final-state interactions in which the pions scatter strongly. The last contribution makes the cross section for $\gamma\gamma \to \pi^0\pi^0$ nonzero, although the magnitude is much smaller than for $\gamma\gamma \to \pi^+\pi^-$.

The QED low-energy theorem requires that $\mathcal{A}(s,t) \to \mathcal{B}(s,t)$ as s approaches the $\pi\pi$ threshold from above. It is expected that $\mathcal{B}$ controls the size of the cross section at $\gamma\gamma$ center-of-mass energies $\sqrt{s} = W < 0.6$ GeV. At higher W values, the effect of all the other exchanges included in $\mathcal{C}$ has to be determined by experiment, pending an exact QCD calculation.

The amplitude $\mathcal{D}$ can be related by unitarity to $\pi\pi \to \pi\pi$ scattering data. Unitarity tells us that for each spin J and isospin I:

$$\mathrm{Im}\mathcal{T}(\pi\pi \to \pi\pi) = \sum_i \rho_i \mathcal{T}(\pi\pi \to i)^* \mathcal{T}(i \to \pi\pi) , \tag{2}$$

where the sum extends over all possible intermediate states i, and the ρ_i are phase-space factors. Below the $K\bar{K}$ threshold and where 4π and 6π channels can be neglected, the only contributing intermediate state is $\pi\pi$ itself. This yields, for $\gamma\gamma \to \pi\pi$:

$$\mathrm{Im}\mathcal{A}(\gamma\gamma \to \pi\pi) = \left[\frac{W^2 - 4m_\pi^2}{W^2}\right]^{1/2} \mathcal{A}(\gamma\gamma \to \pi\pi)^* \mathcal{T}(\pi\pi \to \pi\pi) , \tag{3}$$

implying that the phase of $\mathcal{A}$ is constrained to equal the phase of the $\pi\pi \to \pi\pi$ scattering amplitude with the same quantum numbers. This is expressed by Watson's theorem.[9] Thus using the measured $\pi\pi$ scattering phase shifts and neglecting $\mathcal{C}$ (i.e., exchanges other than π exchange) allows a reliable prediction of the cross section for $\gamma\gamma \to \pi^0\pi^0$ for $W < 0.6$ GeV. For higher masses, $\mathcal{C}$ can no longer be neglected and applying Watson's theorem becomes more complicated since intermediate states other than $\pi\pi$ (e.g., $K\bar{K}$, 4π, 6π, and $\eta\eta$) have to be taken into account. In addition, the Born approximation will overestimate the amplitude for the production of the initial pion pair with increasing W because pions are not pointlike. Taking the pion form factor into account could lead to a solution of this problem.[5]

This paper presents an analysis[10] of the reaction

$$e^+e^- \to e^+e^-\gamma^*\gamma^* \to e^+e^-\pi^0\pi^0 \to e^+e^-\gamma\gamma\gamma\gamma ,$$

which has been used to measure the cross section for $\gamma\gamma \to \pi^0\pi^0$ over the $\pi^0\pi^0$ mass range from threshold to about 2 GeV. The data were collected using the Crystal Ball detector at the DESY e^+e^- storage ring DORIS II at an average beam energy of 5.3 GeV. They represent an integrated luminosity of $\mathcal{L}_{ee} = 97$ pb^{-1} and have been taken with a special low energy threshold trigger. This trigger enables us to observe low-mass final states in which the leptons scatter at very small angles and are not observed in the detector. Therefore, it is necessary to measure the momenta of all particles in the $\pi^0\pi^0$ final state. An event's two-photon origin is ensured by a cut on the total transverse momentum with respect to the beam axis, also effectively restricting the colliding photons γ^* to be nearly real ("quasireal").

DETECTOR AND TRIGGER

The Crystal Ball[11,12] is a nonmagnetic detector well suited to measure the energies and directions of electromagnetically showering particles. Its main part, the calorimeter, consists of a spherical array of 672 NaI(Tl) crystals with 16 radiation lengths (r.l.) each, covering 93% of the solid angle. The crystal arrangement is based on the geometry of an icosahedron. Each of its 20 triangular faces ("major triangles") is divided into four "minor triangles," each consisting of nine individual

crystals; see Fig. 1. Each crystal is shaped like a truncated triangular pyramid pointing towards the interaction point and is viewed by a photomultiplier. Two holes, from omitting two groups of 24 crystals each, allow the beam pipe to pass through the calorimeter. The groups of 30 crystals adjacent to each of the two holes are called the "tunnel crystals." The remaining 612 crystals, covering 85% of 4π sr, make up the "main ball." The solid-angle coverage of the calorimeter is enlarged to 98% of 4π sr by additional hexagonal NaI(Tl) end-cap crystals. In this analysis the end caps are used to reject events not fully contained in the ball.

Electromagnetic showers in the ball are measured with an energy resolution of $\sigma_E/E=(2.7\pm0.2)\%/[E\ (\mathrm{GeV})]^{1/4}$. About 98% of the shower energy is distributed among a group of 13 neighboring crystals with a characteristic lateral pattern that helps in identifying photons and electrons. Using this pattern, we measure shower directions with a resolution in θ, the polar angle with respect to the beam axis, of $\sigma_\theta=3°$–$2°$ for energies in the range 50–500 MeV. The crystals in the ball are calibrated using large-angle Bhabha-scattering events. We found it necessary to correct the calibration at lower energies. From our studies of the process $\Upsilon(2S)\rightarrow\pi^0\pi^0\Upsilon(1S)$, we derived a one-parameter, nonlinear expression, which gives an energy correction of +5% at 100 MeV (Ref. 13).

To detect charged particles, the central cavity of the ball is equipped with four double-layered chambers of proportional tubes that are operated with a (79-20-1)% Ar-CO_2-CH_4 mixture. The chambers surround the beam pipe cylindrically and cover between 98% (chamber 1) and 78% (chamber 4) of the solid angle. Each chamber has a thickness corresponding to 0.017 r.l., the beam pipe adding another 0.017 r.l.

The trigger used in this analysis is based on fast analog sums of the total energy deposited in the main ball, each of its major triangles, each group of tunnel crystals, and on signals from the chambers. Energy sums and chamber signals are subjected to pulse-height discriminators. Accepted events satisfy the following requirements.

(1) *Total energy*: more than 200 MeV.

(2) *Topology*: at least one major triangle with more than 40 MeV in each of the six hemispheres that result from dividing the ball by three different planes which contain the beam axis.[12] Events with badly unbalanced transverse momentum fail this requirement.

(3) *Tunnel energy*: less than 30 MeV in each group of tunnel crystals.

(4) *Chamber veto*: no hit in chamber 3. For about 35% of the data sample, chamber 2 was also required to have no hit.

The energy values quoted above indicate 90% efficiency for individual trigger elements and 10% efficiency for the tunnel energy veto. Energy sums for the main ball and each of the major triangles always exclude tunnel crystals.

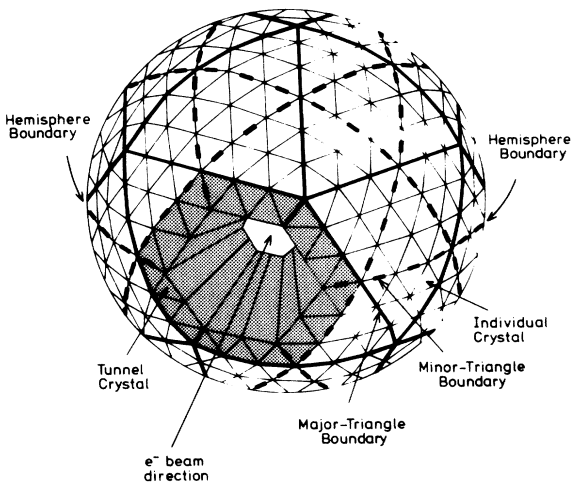

FIG. 1. Organization of the individual crystals into major and minor triangles, and into top and bottom hemispheres. The shaded area shows one group of tunnel crystals.

EVENT SELECTION AND BACKGROUND SUBTRACTION

All events used in this analysis are first passed through a preliminary selection designed to identify candidates for events originating from the collision of two quasireal photons. Events are required to have a total invariant mass of less than 5 GeV and a total transverse momentum $|\sum \mathbf{p}_t|$ of less than 0.2 GeV. At this stage of the analysis, invariant mass and total transverse momentum are calculated by assigning a momentum vector to each crystal with magnitude equal to the energy detected in that crystal.

Out of the preselected events, candidate events for the four-photon final state have been selected by the following criteria.

(i) There must be exactly four clearly separated clusters of energy of at least 30 MeV each, which are considered as photon candidates.

(ii) All photons must be within $|\cos\theta|<0.8$, where θ is a photon's polar angle with respect to the beam axis.

(iii) The lateral energy deposition pattern of each photon must be consistent with that expected for an electromagnetically showering particle originating near the e^+e^- interaction point.

(iv) The total energy deposited in the ball must be less than 3.5 GeV. The total energy seen in all end-cap crystals must be less than 50 MeV. These cuts reject e^+e^- annihilation events and events with additional particles close to the beam.

(v) The energy in the ball that is not associated with the four photon showers ("uncorrelated energy") must not exceed 15 MeV $+0.03\sum_{i=1}^{4}E^{(i)}_{\mathrm{photon}}$, where for this purpose the photon energy has been calculated as the energy sum in 13 crystals without any further corrections. The cut values are chosen to allow for some low-energy beam related background and to account for the energy leaking out of the group of 13 crystals.

(vi) The total transverse momentum squared $|\sum \mathbf{p}_t|^2$ now calculated from the momenta of the four photons has to be less than 0.008 $\mathrm{GeV}^2\times m_{4\gamma}/\mathrm{GeV}$. A mass-

dependent cut has been chosen to achieve a nearly constant cut efficiency over the whole 4γ invariant-mass range. Events failing this cut have been kept to study the $|\sum \mathbf{p}_t|^2$ distribution.

(vii) There must be no tracks in the chambers.

(viii) Events are removed when there are chamber hits closely matched in the azimuth angle around the beam axis with the direction of a photon. The θ information is ignored for this cut because the main background comes from beam-gas and beam-wall interactions that did not necessarily originate at the e^+e^- interaction point. Note that the trigger had already required no hit at all in chamber 3.

(ix) The events must satisfy a software trigger filter with thresholds set to energy values where the hardware is fully efficient. These values are typically 5 to 10 MeV above (below for vetoes) the ones quoted in the trigger description.

We then group the four photons into two pairs (there are three combinations in doing so) and make scatter plots of one pair mass versus the other in various intervals of the 4γ invariant mass (see Fig. 2). We observe strong peaks from $\pi^0\pi^0$ events in all intervals and clusters from $\pi^0\eta$ events in all intervals above the corresponding threshold. We see no clusters from $\eta\eta$ events.[14]

To select $\pi^0\pi^0$ events we require at least one combination with

$$(m_{\gamma\gamma}^{(1)} - m_{\pi^0})^2 + (m_{\gamma\gamma}^{(2)} - m_{\pi^0})^2 < R^2 , \quad (4)$$

which is a circular disk around the $\pi^0\pi^0$ point. The radius R is given by 3σ of our expected mass resolution for π^0's. Using Monte Carlo events, the π^0 mass resolution has been determined as a function of the 4γ invariant mass. It rises from $\sigma = 7.5$ MeV at $m_{4\gamma} = 0.3$ GeV to $\sigma = 12.5$ MeV at $m_{4\gamma} = 1.5$ GeV. To suppress $\pi^0\eta$ and possible $\eta\eta$ events, we perform a χ^2 test of the three hypotheses $\pi^0\pi^0$, $\pi^0\eta$, and $\eta\eta$, and finally classify the events according to the highest confidence level (C.L.). Note that the events are not kinematically fit to the $\pi^0\pi^0$ hypothesis. For 4γ invariant masses below 0.5 GeV, about 15% of the $\pi^0\pi^0$ events have two combinations satisfying Eq. (4); for higher 4γ invariant masses this fraction is negligible. For the remainder of the analysis, we consider only the most likely combination, the one with the highest C.L. Figure 3 shows the invariant-mass distribution of the selected 1574 $\pi^0\pi^0$ events; it exhibits a dominant peak due to the formation of the $f_2(1270)$ resonance.

The $|\sum \mathbf{p}_t|^2$ distribution of the $\pi^0\pi^0$ events peaks at zero as expected for two-photon produced events (see below). However, for low $\pi^0\pi^0$ invariant masses we observe an excess of events with high $|\sum \mathbf{p}_t|^2$ values. The source of this background is most likely $\pi^0\pi^0$ production in beam-gas reactions. To study it, we use a sample of data taken with a single e^+ or e^- beam, or with the e^+ and e^- beam separated. These beam-gas data correspond to an integrated luminosity of 6.0 ± 0.6 pb^{-1}. This is the same data sample as used in Ref. 12, where a corresponding background has been observed for the two-photon production of single π^0's. Applying the selection criteria described above, except for the $|\sum \mathbf{p}_t|^2$ cut, results in 26 $\pi^0\pi^0$ events from the beam-gas sample. Their invariant-mass distribution [Fig. 4(a)] shows that this background contributes only at low $\pi^0\pi^0$ invariant masses and becomes negligible for $m_{\pi^0\pi^0}$ above 0.9 GeV. The $|\sum \mathbf{p}_t|^2$ distribution of these events [Figure 4(b)] does not peak at zero but is fairly flat.

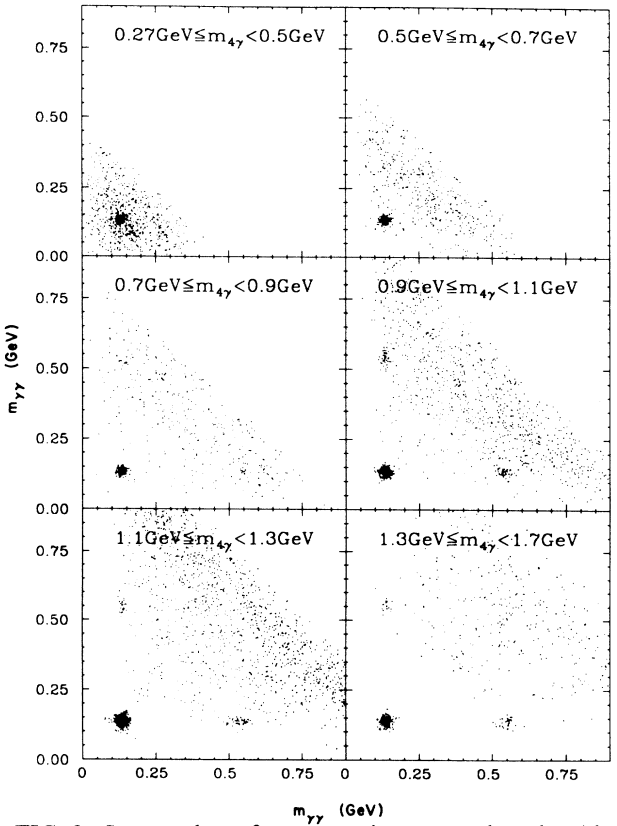

FIG. 2. Scatter plots of one $\gamma\gamma$ pair mass vs the other (three entries per event) for various intervals of the 4γ invariant mass.

Since only three of the $\pi^0\pi^0$ beam-gas events pass the (mass-dependent) $|\sum \mathbf{p}_t|^2$ cut, it is not appropriate to use their luminosity scaled invariant-mass distribution to correct Fig. 3 for this background. Instead, we apply the

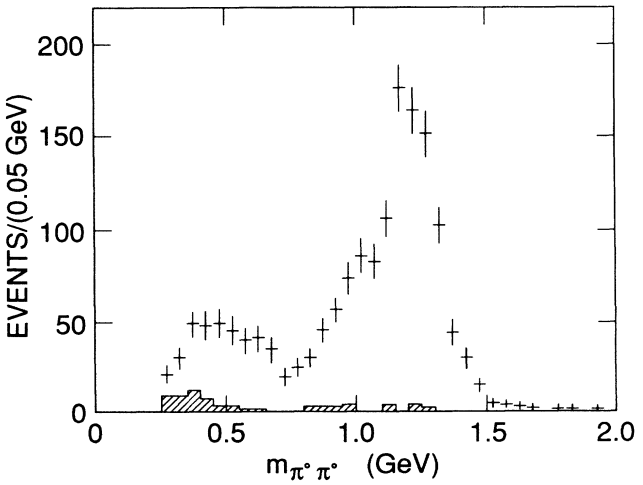

FIG. 3. Invariant-mass distribution of the selected $\pi^0\pi^0$ events. The shaded histogram shows the background as determined from fits to the $|\sum \mathbf{p}_t|^2$ distributions.

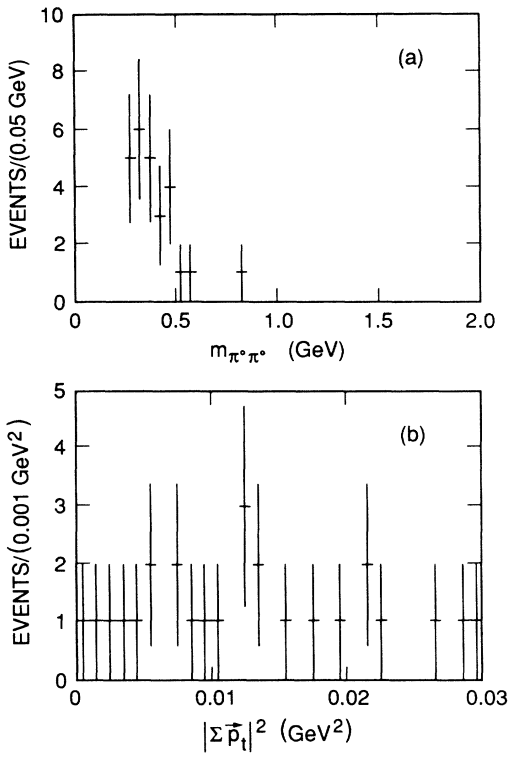

FIG. 4. (a) Invariant-mass distribution of $\pi^0\pi^0$ events from the beam-gas sample. The $|\sum \mathbf{p}_t|^2$ cut has not been applied to these events. (b) $|\sum \mathbf{p}_t|^2$ distribution of $\pi^0\pi^0$ events from the beam-gas sample.

following procedure to the events from the colliding-beam sample. For the $\pi^0\pi^0$ events in each single mass bin, we fit the $|\sum \mathbf{p}_t|^2$ distribution to the Monte Carlo expectation[15] for $\gamma\gamma \to \pi^0\pi^0$ plus a straight line describing the beam-gas background. (See Fig. 5 for some typical fits.) From the straight line we deduce the number of

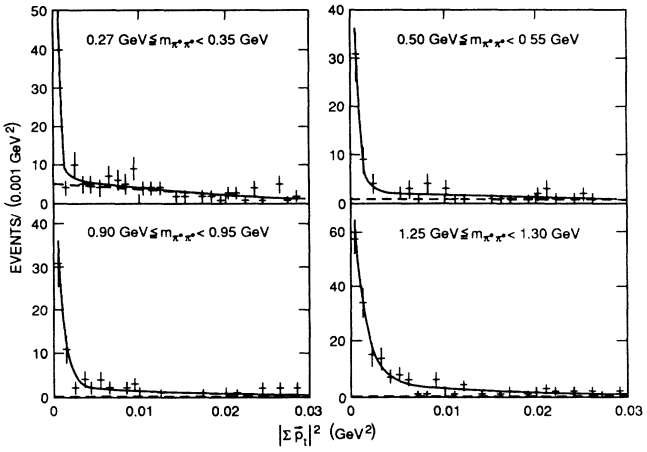

FIG. 5. $|\sum \mathbf{p}_t|^2$ distributions for $\pi^0\pi^0$ events from the colliding-beam sample in some selected intervals of the $\pi^0\pi^0$ invariant mass. Also shown are the fits to the distributions with a sum (solid line) of the Monte Carlo expectation for $\gamma\gamma \to \pi^0\pi^0$ and a straight line (dashed line) describing the beam-gas background.

background events passing the $|\sum \mathbf{p}_t|^2$ cut. The shaded histogram in Fig. 3 shows the background contribution as a function of the $\pi^0\pi^0$ invariant mass. This procedure yields 39 ± 4 background events for $m_{\pi^0\pi^0} < 0.9$ GeV. This is in agreement with the expectation of 49 ± 28 events we would obtain from the beam-gas sample by scaling the three observed events to the luminosity of the colliding-beam sample.

MONTE CARLO SIMULATION AND EFFICIENCY DETERMINATION

To obtain the total cross section $\sigma_{\gamma\gamma}$ for $\gamma\gamma \to \pi^0\pi^0$, the background-subtracted $\pi^0\pi^0$ invariant-mass distribution has to be corrected for the W-dependent $\gamma\gamma$ luminosity and the detection efficiency, where W is the invariant mass of the $\gamma\gamma$ and $\pi^0\pi^0$ system.

For each W bin, the $\gamma\gamma$ flux $\mathcal{F}_{\gamma\gamma}(W)$ (i.e., the ratio of the $\gamma\gamma$ luminosity to the e^+e^- luminosity) has been calculated by a numerical integration of the flux formula given in Ref. 15, taking into account only transverse photons.

To determine the detection efficiency, we have generated events of the type $e^+e^- \to e^+e^-\pi^0\pi^0 \to e^+e^-\gamma\gamma\gamma\gamma$ using the same formula from Ref. 15. These events have been passed through a detailed detector-simulation program based on the shower-development code EGS 3 (Ref. 16). Some of the selection criteria, especially the cuts on end-cap energy, uncorrelated energy, and tunnel veto energy, are affected by extra energy deposited in the calorimeter by beam-related background. This extra energy was accounted for by using a sample of random background events obtained by triggering on every 10^7 beam crossing, with no other condition. A different background event was superimposed on each Monte Carlo event. The Monte Carlo events were then passed through the same analysis chain as the real data, except for any cuts on chamber information.

The efficiency of the selection criteria based on chamber information varies with chamber performance. It was therefore not calculated by Monte Carlo methods but has been determined using the data itself. From data taken with triggers that had no chamber veto, we select $\gamma\gamma \to \pi^0\pi^0$ events in the $f_2(1270)$ region. The selection uses cuts looser than the ones described above and makes no use of the chamber information. It yields a sample of about 1900 $f_2(1270)$ events with negligible background. This sample, divided into periods of similar chamber performance, has been used to determine an average efficiency $\epsilon_{\rm ch}$ of $(69.4\pm1.3)\%$ for a $\pi^0\pi^0$ event to pass the chamber veto and the cuts on hits in the chambers. The inefficiency is due to photons converting in the beam pipe or in the chamber material and to noise hits in the chambers. Monte Carlo studies show that $\epsilon_{\rm ch}$ is almost constant over the entire $\pi^0\pi^0$ invariant-mass range. We do not correct for its slight mass dependence but include the effect in the systematic error on $\sigma_{\gamma\gamma}$.

To determine $\sigma_{\gamma\gamma}$ independent of any assumptions on the spin and helicity state of the $\pi^0\pi^0$ system, we have divided the Monte Carlo–generated events into bins of $\Delta W = 0.05$ GeV and $\Delta|\cos\theta^*| = 0.1$, where θ^* is the an-

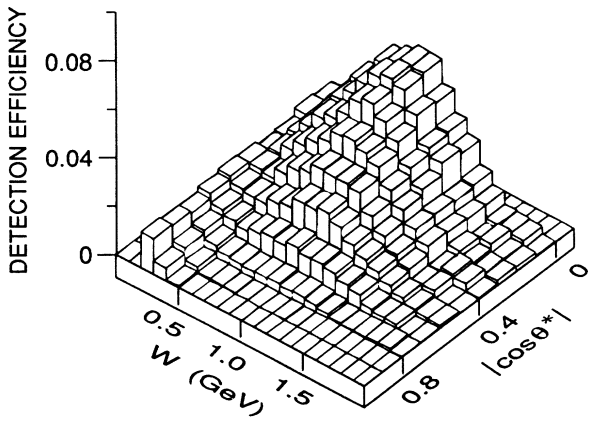

FIG. 6. Detection efficiency as a function of W and $|\cos\theta^*|$.

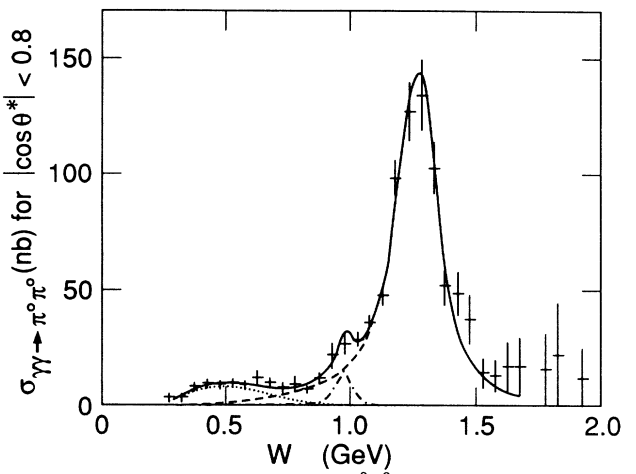

FIG. 7. Cross section for $\gamma\gamma\to\pi^0\pi^0$ as a function of W for $|\cos\theta^*|<0.8$. The solid line is the result of a fit with $f_2(1270)$ (dashed line), $f_0(975)$ (dashed-dotted line), and nonresonant continuum contributions (dotted line).

gle between the beam axis and one of the π^0's in the $\gamma\gamma$ center-of-mass system (c.m.s.). Calculating for each bin the ratio of accepted to generated events results in a two-dimensional efficiency matrix. The efficiency $\epsilon_{\rm MC}(W,|\cos\theta^*|)$ is maximal for W near 1 GeV and $|\cos\theta^*|$ near zero, dropping considerably towards lower and higher W and higher $|\cos\theta^*|$ values as shown in Fig. 6. In order to keep the statistical error on $\epsilon_{\rm MC}$ reasonably small in each cell, the $|\cos\theta^*|$ range used below to calculate $\sigma_{\gamma\gamma}$ was restricted to $|\cos\theta^*|<0.8$.

To check contributions from other two-photon processes, Monte Carlo events of the types $\gamma\gamma\to\{\eta,\eta',\ a_2(1320)$, and $\pi_2(1680)\}$ have been generated with two-photon widths taken from Refs. 17 and 18. After a complete detector simulation the events were subjected to the cuts described above except for the cuts on chamber information. We find only negligible contributions from all of the channels considered (11.9±1.4 events total).

TOTAL CROSS SECTION FOR $\gamma\gamma\to\pi^0\pi^0$

The total cross section $\sigma_{\gamma\gamma}$ vs W has been calculated by weighting each event with

$$[\mathcal{L}_{ee}\mathcal{F}_{\gamma\gamma}(W)\epsilon_{\rm MC}(W,|\cos\theta^*|)\epsilon_{\rm ch}]^{-1}\ .$$

After subtracting the background fractions determined previously, we obtain the cross section for $\gamma\gamma\to\pi^0\pi^0$ as a function of W for $|\cos\theta^*|<0.8$; see Fig. 7, and Table I. Between threshold and about 0.8 GeV, $\sigma_{\gamma\gamma}$ is fairly flat and about 10 nb. At higher invariant masses the $f_2(1270)$ resonance dominates, and we observe a hint of the $f_0(975)$.

The systematic error on $\sigma_{\gamma\gamma}$ is 11% for $W<0.8$ GeV and 7% for $W>0.8$ GeV. It includes the following contributions, all added in quadrature: uncertainty in the e^+e^- integrated luminosity (±4%), uncertainty in the $\gamma\gamma$ flux determination and effect of neglecting a ρ-pole form factor (±2%), variation of cuts, uncertainties in the

TABLE I. Total cross section for $\gamma\gamma\to\pi^0\pi^0$ for $|\cos\theta^*|<0.8$. The W values listed are the bin centers. The quoted errors are statistical only. A systematic error of 11% for $W<0.8$ GeV and of 7% for $W>0.8$ GeV has to be added.

W (GeV)	$\sigma(\gamma\gamma\to\pi^0\pi^0)$ (nb)	W (GeV)	$\sigma(\gamma\gamma\to\pi^0\pi^0)$ (nb)
0.275	3.8±1.1	1.075	35.4±4.5
0.325	3.8±0.9	1.125	47.2±5.1
0.375	8.2±1.6	1.175	98.0±8.3
0.425	9.5±1.8	1.225	126.3±12.8
0.475	8.7±1.5	1.275	133.4±15.5
0.525	9.7±1.7	1.325	102.0±11.3
0.575	8.6±1.7	1.375	51.6±8.5
0.625	12.1±2.9	1.425	47.8±9.3
0.675	9.6±2.0	1.475	36.6±10.2
0.725	7.5±2.7	1.525	14.1±6.6
0.775	9.1±3.9	1.575	13.0±6.7
0.825	7.3±1.4	1.625	16.9±10.5
0.875	11.9±2.1	1.675	16.6±13.0
0.925	21.7±5.4	1.775	15.7±15.7
0.975	26.7±4.7	1.825	21.8±21.8
1.025	28.3±3.4	1.925	12.1±12.1

calculation of ϵ_{MC} and in the background subtraction ($\pm 8\%$ for $W<0.8$ GeV and $\pm 4\%$ for $W>0.8$ GeV), and uncertainties in the calculation of ϵ_{ch} and its extrapolation to low $\pi^0\pi^0$ invariant masses ($\pm 6\%$ for $W<0.8$ GeV and $\pm 4\%$ for $W>0.8$ GeV).

The cross section we measure at low $\pi^0\pi^0$ invariant masses can be compared to the prediction from the unitarized Born-term model described in the Introduction. Using the ansatz $\mathcal{A}=\mathcal{B}+\mathcal{D}$ (i.e., neglecting $\mathcal{C}$) and taking the $I=0,2$, $J=0$ $\pi\pi$ scattering phase shifts to determine $\mathcal{D}$ results in the prediction[8] shown by the solid line in Fig. 8. It is in remarkable agreement with the data for $W<0.6$ GeV. The disagreement at higher masses can be attributed to neglecting $\mathcal{C}$. Attempts to describe the DM1/2 measurement of $\gamma\gamma\to\pi^+\pi^-$ lead to a predicted cross section for $\gamma\gamma\to\pi^0\pi^0$ which, close to threshold, is as large as 100 nb (Refs. 8 and 19), in total disagreement with our data. Work is in progress[20] to apply the model in Ref. 8 up to masses above the $f_2(1270)$ and to simultaneously fit $\gamma\gamma\to\pi^+\pi^-$ and $\gamma\gamma\to\pi^0\pi^0$ data, which are related by isospin invariance.

The cross section for the formation of a scalar ($J^{PC}=0^{++}$) or tensor ($J^{PC}=2^{++}$) resonance R in quasi-real two-photon collisions and its subsequent decay into $\pi^0\pi^0$ can be described by a relativistic Breit-Wigner form:

$$\sigma_{\gamma\gamma\to R\to\pi^0\pi^0}(W) = 8\pi(2J+1)\left[\frac{m}{W}\right]^2 \frac{\Gamma_{\gamma\gamma}B(R\to\pi^0\pi^0)\Gamma_{\rm tot}(W)}{(W^2-m^2)^2+m^2\Gamma_{\rm tot}^2(W)}, \quad (5)$$

where J denotes the spin of the resonance, m its mass, $\Gamma_{\rm tot}$ its total width, and $B(R\to\pi^0\pi^0)$ its branching ratio into $\pi^0\pi^0$. This Breit-Wigner form follows from the helicity-amplitude decomposition given in Ref. 5. In case of the tensor resonance, only the helicity-2 amplitude is assumed to contribute to the cross section. The W dependence of $\Gamma_{\rm tot}$ is parametrized according to Ref. 21:

$$\Gamma_{\rm tot}(W)=\Gamma_{\rm tot}(m)\frac{m}{W}\left[\frac{q^*}{q_0^*}\right]^{2L+1}\frac{D_L(q_0^*r)}{D_L(q^*r)}, \quad (6)$$

where $q^*(W)$ is the π^0 momentum in the $\gamma\gamma$ c.m.s.,

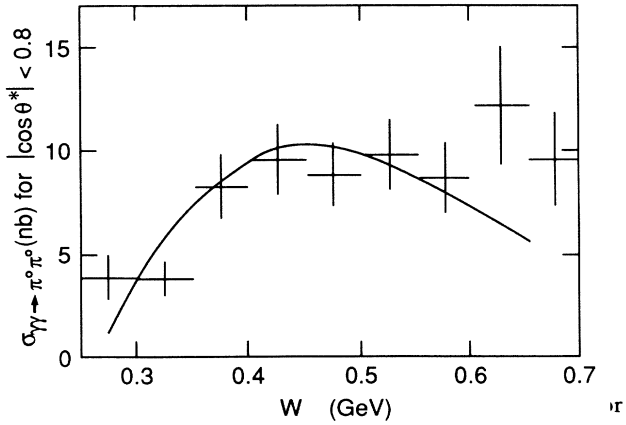

FIG. 8. Cross section for $\gamma\gamma\to\pi^0\pi^0$ as a function of W for $W<0.7$ GeV and $|\cos\theta^*|<0.8$. Also shown is the prediction (solid line) from the model in Ref. 8.

$q_0^*=q^*$ ($W=m$), and $L=J$ for a decay into spinless particles. The decay form factors D_L are given by Ref. 22:

$$D_0=1 \text{ and } D_2(W)=9+3(q^*r)^2+(q^*r)^4, \quad (7)$$

and the effective interaction radius r is assumed to be 1 fm.

We fit[23] the cross section to a sum of three incoherent contributions (solid line in Fig. 7).

(1) A phenomenological curve of the form $(W-2m_{\pi^0})^a e^{-W/b}$, with free parameters a and b to account for $\pi^0\pi^0$ continuum production (dotted line). Note that for $W<0.6$ GeV the shape of this curve is very similar to the unitarized Born-term model prediction[8] shown in Figure 8.

(2) A relativistic spin-0 Breit-Wigner form with mass $m=0.975$ GeV and total width $\Gamma_{\rm tot}(m)=0.033$ GeV for the $f_0(975)$, folded with a Gaussian mass resolution ($\sigma=0.020$ GeV), with $\Gamma_{\gamma\gamma}(f_0(975))$ as a free parameter (dashed-dotted line).

(3) A relativistic spin-2 Breit-Wigner form for the $f_2(1270)$, folded with a Gaussian mass resolution ($\sigma=0.028$ GeV), with m, $\Gamma_{\rm tot}(m)$, and $\Gamma_{\gamma\gamma}(f_2(1270))$ as free parameters (dashed line).

The fit yields, for the $f_2(1270)$ (statistical errors only),

$$m=1.274\pm 0.006 \text{ GeV}$$

and (8)

$$\Gamma_{\rm tot}(m)=0.178\pm 0.015 \text{ GeV},$$

in good agreement with the Particle Data Group (PDG) values.[17] Our result also agrees with a preliminary JADE measurement[24] of the reaction $\gamma\gamma\to\pi^0\pi^0$. Neither experiment observes a downward shift of the $f_2(1270)$ peak as it is measured in the reaction $\gamma\gamma\to\pi^+\pi^-$ (Ref. 25). A previous measurement from the Crystal Ball at the SLAC e^+e^- storage ring SPEAR (Ref. 26) yielded $m=1.238\pm 0.014\pm 0.025$ GeV (statistical and systematic error) and $\Gamma_{\rm tot}(m)=0.248\pm 0.038$ GeV (statistical error only). This mass measurement is 1.2 standard deviations (s.d.) away from the PDG value and the shift is not considered to be statistically significant.

In a separate fit the $f_0(975)$ mass and total width are also free parameters. This fit yields for the $f_0(975)$ (statistical errors only): $m=0.980\pm 0.028$ GeV and $\Gamma_{\rm tot}(m)=0.050\pm 0.037$ GeV, in good agreement with the PDG values. The value of $\Gamma_{\gamma\gamma}(f_0(975))$ does not change significantly; however, its error increases considerably.

To determine their two-photon widths, we assume isotropy for the $f_0(975)$ decay and pure helicity 2 for the $f_2(1270)$ decay in correcting for the unmeasured part of the cross section beyond $|\cos\theta^*|=0.8$. The validity of these assumptions will be discussed below. Taking into account the branching ratios[17] $B(f_2(1270)\to\pi^0\pi^0)=\frac{1}{3}\times(86^{+2}_{-1})\%$ and $B(f_0(975)\to\pi^0\pi^0)=\frac{1}{3}\times(78\pm 3)\%$, we measure

$$\Gamma_{\gamma\gamma}(f_2(1270))=3.19\pm 0.16\pm^{0.29}_{0.28} \text{ keV},$$
$$\Gamma_{\gamma\gamma}(f_0(975))=0.31\pm 0.14\pm 0.09 \text{ keV}, \quad (9)$$

TABLE II. Comparison of our results with other measurements of $\Gamma_{\gamma\gamma}(f_2(1270))$ and $\Gamma_{\gamma\gamma}(f_0(975))$. Also shown are the two-photon widths of other tensor and scalar mesons. Statistical and systematic errors have been added in quadrature.

Particle	$\Gamma_{\gamma\gamma}$ (keV)	Reference
$f_2(1270)$	$3.19\pm^{0.33}_{0.32}$	This experiment
	2.76±0.14	PDG (Ref. 17)
$a_2(1320)$	0.90±0.11	PDG (Ref. 17)
$f_2'(1525)$	0.11±0.04	PDG (Ref. 17)
$f_0(975)$	0.31±0.17	This experiment
	0.24±0.16	Mark II (Ref. 29)
$a_0(980)$	$0.19\pm^{0.12}_{0.10}$	Crystal Ball (Ref. 30)
	0.29±0.15	JADE (Ref. 24)

where the errors are statistical and systematic, respectively. This result is obtained with a fixed $f_0(975)$ mass and total width in the fit. In addition to the systematic errors on $\sigma_{\gamma\gamma}$ quoted above, the systematic errors on the two-photon widths take into account the following contributions, all added in quadrature: uncertainties in the branching ratios into $\pi^0\pi^0$ leading to $\pm^{0.08}_{0.04}$ keV for the $f_2(1270)$ and ±0.01 keV for the $f_0(975)$; uncertainty in the parametrization of the $f_2(1270)$ Breit-Wigner form leading to ±0.15 keV for the $f_2(1270)$ and ±0.09 keV for the $f_0(975)$. The value of the effective interaction radius r determines the size of the low-mass tail of the $f_2(1270)$, on which the value we obtain for $\Gamma_{\gamma\gamma}(f_0(975))$ depends crucially. r has been varied between 0.5 fm and 1.5 fm. The uncertainty in the parametrization of the $f_0(975)$ itself has a negligible effect.

The value we obtain for $\Gamma_{\gamma\gamma}(f_2(1270))$ is in good agreement with the average of previous measurements (see Table II). These results, together with the measurements of $\Gamma_{\gamma\gamma}(a_2(1320))$ and $\Gamma_{\gamma\gamma}(f_2'(1525))$ (see Table II), confirm close to ideal mixing and approximate nonet symmetry in the tensor-meson nonet.[27]

Converting our $f_0(975)$ measurement, which has only 2.2 s.d. statistical significance, into an upper limit[28] yields

$$\Gamma_{\gamma\gamma}(f_0(975))<0.53 \text{ keV} \quad \text{at } 90\% \text{ C.L.} \tag{10}$$

However, our central value agrees well with a preliminary Mark II measurement.[29] These measurements, together with results on $\Gamma_{\gamma\gamma}(a_0(980))$ (see Table II), agree well with an interpretation of both states as four-quark states (see Table III).

Our measurements assume that both the $f_0(975)$ and the $f_2(1270)$ can be described by Breit-Wigner forms, and that the underlying continuum is smooth. As has been pointed out recently,[8] this fit ansatz is oversimplified since it neglects the opening of the strongly coupled $K\bar{K}$ channel and ignores the constraints from the $\pi\pi$ phase shifts. However, lacking a procedure that meets these requirements, we use the standard Breit-Wigner approach.

The data presented do not allow us to thoroughly investigate $\pi^0\pi^0$ production in the mass region well above the $f_2(1270)$. Since this analysis aimed for a cross-section measurement down to $\pi^0\pi^0$ threshold, it used

TABLE III. Some theoretical predictions for the two-photon widths of $f_0(975)$ and $a_0(980)$. θ_S denotes the octet-singlet mixing angle in the scalar nonet.

Model	$\Gamma_{\gamma\gamma}(f_0(975))$ (keV)	$\Gamma_{\gamma\gamma}(a_0(980))$ (keV)	Reference
$q\bar{q}$	5.0	1.8	NRQM[a]
$q\bar{q}$		2.5–3.8	Ref. 31
$q\bar{q}$		0–0.37	Ref. 32
$q\bar{q}$	$12.8\left[\sin\theta_S-\frac{1}{\sqrt{8}}\cos\theta_S\right]^2$	4.8	Ref. 33
$q\bar{q}$	3.0	1.1	Ref. 34
$q\bar{q}$		0.6	Ref. 35
$q^2\bar{q}^2$	~0.27	~0.27	Ref. 36
$K\bar{K}$ molecule	0.6	0.6	Refs. 34 and 37

[a]In the nonrelativistic quark model (NRQM) one may relate the two-photon widths of scalar and tensor states having identical flavor content and spatial wave functions through a spin and a phase-space factor (Ref. 34):

$$\Gamma_{\gamma\gamma}(q\bar{q}(0^{++}))=\frac{15}{4}\left[\frac{m(0^{++})}{m(2^{++})}\right]^3\Gamma_{\gamma\gamma}(q\bar{q}(2^{++}))\ .$$

Taking the average of $\Gamma_{\gamma\gamma}(f_2(1270))$ from Table II yields

$$\Gamma_{\gamma\gamma}(f_0(975))=5 \text{ keV}\ .$$

Assuming ideal octet-singlet mixing ($\theta_S=35.3°$) results in the relation

$$\Gamma_{\gamma\gamma}(a_0(980))=\tfrac{9}{25}\Gamma_{\gamma\gamma}(f_0(975))=1.8 \text{ keV}\ .$$

The factor $\frac{9}{25}$ is the square of the ratio of the mean squared quark charge of the two states.

only data taken with a low energy threshold trigger (about 40% of the total data sample collected with the Crystal Ball), and the applied selection criteria have low efficiency in the high-mass regime. Yet we can exclude a dramatic rise of the cross section in the region between the $f_2(1270)$ and about 2 GeV.

DIFFERENTIAL CROSS SECTION $d\sigma/d|\cos\theta^*|$

The extrapolation to the full $|\cos\theta^*|$ range, which we used above in determining $\Gamma_{\gamma\gamma}$, results from investigating the decay angular distributions in the $\gamma\gamma$ c.m.s. Figure 9 shows the background-subtracted differential cross sections $d\sigma/d|\cos\theta^*|$ in various ranges of the $\pi^0\pi^0$ invariant mass; see also Table IV. (From events with $|\sum \mathbf{p}_t|^2 > 0.05$ GeV^2, we find the $|\cos\theta^*|$ distribution of the background to be flat. This has been used in getting the background-subtracted differential cross sections.)

The differential cross sections can be described by a coherent sum of spherical harmonics $Y_{J\lambda}(\cos\theta^*,\phi^*)$ with complex coefficients $a_{J\lambda}$, where $Y_{J\lambda}$ is the spherical harmonic for orbital momentum J and helicity λ:

$$\frac{d\sigma}{d|\cos\theta^*|} = 2\int_0^{2\pi} d\phi^* |a_{00}Y_{00} + a_{20}Y_{20} + a_{22}Y_{22}|^2$$
$$= 4\pi(|a_{00}|^2|Y_{00}|^2 + |a_{20}|^2|Y_{20}|^2 + |a_{22}|^2|Y_{22}|^2 + |a_{00}||a_{20}|\cos\delta Y_{00}Y_{20}) . \quad (11)$$

Contributions with $J=1$ or $\lambda=1$ have been omitted because of the restrictions for quasireal photons as described by the Landau-Yang theorem.[38] Allowing for interference between the considered contributions introduces as an additional degree of freedom the phase angle δ. (There is only one phase angle since the other interference terms vanish after integrating over ϕ^*.) However, it is not possible to determine simultaneously the $a_{J\lambda}$ and δ from a fit to $d\sigma/d|\cos\theta^*|$. Given this limitation, we follow the standard practice and fit the differential cross sections to a sum (full lines in Fig. 9) of $|Y_{00}|^2$ (dotted lines), $|Y_{20}|^2$ (dashed-dotted lines), and $|Y_{22}|^2$ (dashed lines); see also Table V.

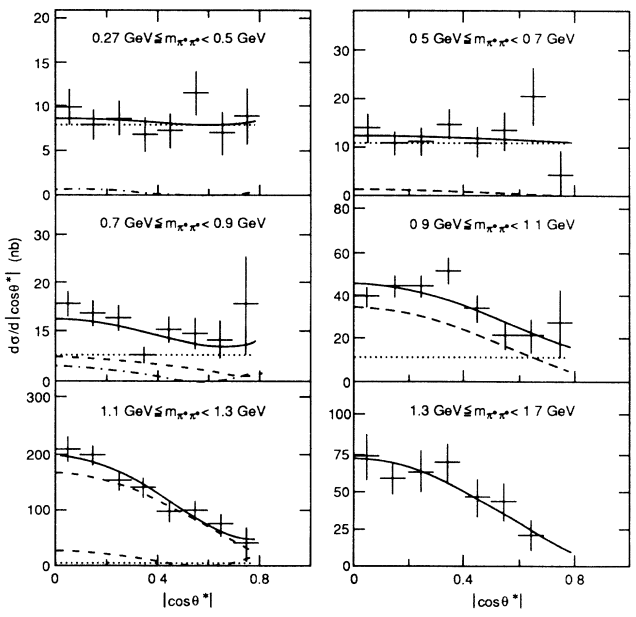

FIG. 9. Differential cross sections $d\sigma/d|\cos\theta^*|$ in various intervals of the $\pi^0\pi^0$ invariant mass. The full line is the result of a fit to the sum of $|Y_{00}|^2$ (dotted line), $|Y_{20}|^2$ (dashed-dotted line), and $|Y_{22}|^2$ (dashed line). Note that the fit yields pure $|Y_{22}|^2$ in the highest-mass interval.

We find the $\pi^0\pi^0$ system to be dominantly spin 0 for $W<0.7$ GeV. In the $f_2(1270)$ region we measure almost entirely spin 2, helicity 2. The spin-2, helicity-0 fraction is small over the entire mass range. In the region around the $f_0(975)$ ($0.9\le W<1.1$ GeV), we observe a spin-0 contribution of about 40% that is consistent with the $f_0(975)$ contribution seen in the fit to the total cross section.

To further investigate the helicity structure of the $f_2(1270)$ and to look for other spin-0 states in the vicinity of the $f_2(1270)$, we apply the same fitting procedure to the combined distribution for $1.1\le W<1.5$ GeV (Fig. 10). We now find pure spin 2, helicity 2 yielding the following upper limits (90% C.L.):

$$\frac{\text{spin 0}}{\text{total}} < 0.19 \quad \text{and} \quad \frac{\text{spin 2, helicity 0}}{\text{total}} < 0.22 . \quad (12)$$

This result confirms the helicity-2 dominance for $f_2(1270)$ formation in quasireal two-photon collisions as expected from theory[32,39] and as already observed by other experiments (see Table VI).

Our upper limit on the spin-0 fraction in the invariant mass range $1.1\le W<1.5$ GeV has been used to determine upper limits on the two-photon width of the $f_0(1300)$ resonance. Assuming $m_{f_0}=1.3$ GeV, we find at 90% C.L.

$$\Gamma_{\gamma\gamma}(f_0(1300))B(f_0(1300)\to\pi^0\pi^0) < \begin{cases} 1.0 \text{ keV} & \text{for } \Gamma_{\text{tot}}(f_0(1300))=0.15 \text{ GeV} , \\ 1.3 \text{ keV} & \text{for } \Gamma_{\text{tot}}(f_0(1300))=0.3 \text{ GeV} , \\ 1.7 \text{ keV} & \text{for } \Gamma_{\text{tot}}(f_0(1300))=0.4 \text{ GeV} . \end{cases} \quad (13)$$

These limits are comparable to a corresponding limit obtained previously by TASSO (Ref. 40) in the $\pi^+\pi^-$ decay channel.

SUMMARY

We have analyzed the reaction $e^+e^-\to e^+e^-\pi^0\pi^0$ using 97 pb^{-1} of data taken with a special low energy threshold trigger. For the first time we have measured the cross section for $\gamma\gamma\to\pi^0\pi^0$ over the $\pi^0\pi^0$ invariant-mass range from threshold to about 2 GeV. We observe an approximately flat cross section of about 10 nb for $W<0.8$ GeV. For $W<0.6$ GeV our measurement is in good agreement with a theoretical prediction based on an unitarized Born-term model, but disagrees with a previous DM1/2 measurement in the isospin related $\pi^+\pi^-$ channel. At masses above 0.8 GeV the cross section is

TABLE IV. Differential cross sections $d\sigma/d|\cos\theta^*|$ in various W ranges. The $|\cos\theta^*|$ values listed are the bin centers. The quoted errors are statistical only.

W range (GeV)	$\lvert\cos\theta^*\rvert$	$d\sigma/d\lvert\cos\theta^*\rvert$ (nb)	$\lvert\cos\theta^*\rvert$	$d\sigma/d\lvert\cos\theta^*\rvert$ (nb)
0.27–0.5	0.05	9.9±1.9	0.45	7.3±2.0
	0.15	7.8±1.7	0.55	11.6±2.6
	0.25	8.6±1.9	0.65	7.0±2.4
	0.35	6.9±1.8	0.75	8.9±3.2
0.5–0.7	0.05	14.1±2.6	0.45	10.9±3.0
	0.15	10.8±2.3	0.55	13.4±4.0
	0.25	11.2±2.5	0.65	20.5±6.3
	0.35	14.7±3.1	0.75	4.6±4.6
0.7–0.9	0.05	15.6±2.5	0.45	10.1±2.7
	0.15	13.5±2.4	0.55	9.6±3.2
	0.25	12.5±2.4	0.65	8.2±3.8
	0.35	5.0±1.6	0.75	15.5±10.3
0.9–1.1	0.05	38.7±5.0	0.45	33.5±6.3
	0.15	43.5±5.3	0.55	21.0±5.6
	0.25	43.4±5.7	0.65	20.9±7.9
	0.35	51.0±6.8	0.75	27.2±15.7
1.1–1.3	0.05	208.6±18.1	0.45	96.8±15.3
	0.15	199.1±18.1	0.55	99.5±17.8
	0.25	152.5±16.1	0.65	73.9±20.7
	0.35	141.0±16.7	0.75	39.6±30.8
1.3–1.7	0.05	72.7±15.4	0.45	46.2±13.3
	0.15	58.2±11.3	0.55	42.5±13.2
	0.25	62.4±13.9	0.65	21.1±9.9
	0.35	69.0±12.4		
1.1–1.5	0.05	161.3±12.4	0.45	82.5±11.4
	0.15	149.4±12.2	0.55	85.4±13.4
	0.25	115.6±10.9	0.65	57.3±13.3
	0.35	131.3±12.9	0.75	21.4±16.3

dominated by the excitation of the $f_2(1270)$ resonance. We also observe a hint of $f_0(975)$ formation. We see no indication for a dramatic rise of the cross section in the mass region between the $f_2(1270)$ and about 2 GeV. From a Breit-Wigner fit we measure the $f_2(1270)$ mass and total width in agreement with their PDG values and deduce the following two-photon widths:

$$\Gamma_{\gamma\gamma}(f_2(1270))=3.19\pm0.16\pm^{0.29}_{0.28}\ \text{keV}\ ,$$

$$\Gamma_{\gamma\gamma}(f_0(975)<0.53\ \text{keV}\ \text{ at 90\% C.L.}$$

The $f_2(1270)$ measurement assumes pure helicity 2. The $f_0(975)$ upper limit is derived from measuring $\Gamma_{\gamma\gamma}(f_0(975))=0.31\pm0.14\pm0.09$ keV.

From investigating the decay angular distribution in the $\gamma\gamma$ c.m.s., we find the $\pi^0\pi^0$ system to be dominantly spin 0 for $W<0.7$ GeV and spin 2, helicity 2 in the $f_2(1270)$ region ($1.1\le W<1.5$ GeV). In the latter region, we measure the following 90%-C.L. upper limits:

$$\frac{\text{spin 0}}{\text{total}}<0.19\ \text{ and }\ \frac{\text{spin 2, helicity 0}}{\text{total}}<0.22\ .$$

TABLE V. Spin-J, helicity-λ fractions, $a_{J\lambda}$, as determined from the fits to the differential cross sections in various W ranges. Note that the sum of all fractions is normalized to one.

W Range (GeV)	$\lvert a_{00}\rvert^2$	$\lvert a_{20}\rvert^2$	$\lvert a_{22}\rvert^2$
0.27–0.5	$0.94\pm^{0.06}_{0.25}$	$0.06\pm^{0.19}_{0.06}$	$0.0\pm^{0.22}_{0.0}$
0.5–0.7	$0.92\pm^{0.08}_{0.27}$	$0.0\pm^{0.15}_{0.0}$	$0.08\pm^{0.27}_{0.08}$
0.7–0.9	$0.54\pm^{0.27}_{0.44}$	$0.22\pm^{0.15}_{0.12}$	$0.24\pm^{0.41}_{0.24}$
0.9–1.1	$0.38\pm^{0.21}_{0.25}$	$0.0\pm^{0.22}_{0.0}$	$0.62\pm^{0.25}_{0.35}$
1.1–1.3	$0.04\pm^{0.17}_{0.04}$	$0.18\pm^{0.15}_{0.13}$	$0.78\pm^{0.13}_{0.22}$
1.3–1.7	$0.0\pm^{0.23}_{0.0}$	$0.0\pm^{0.15}_{0.0}$	$1.0\pm^{0.0}_{0\ 25}$
1.1–1.5	$0.0\pm^{0.15}_{0.0}$	$0.0\pm^{0.18}_{0.0}$	$1.0\pm^{0.0}_{0.27}$

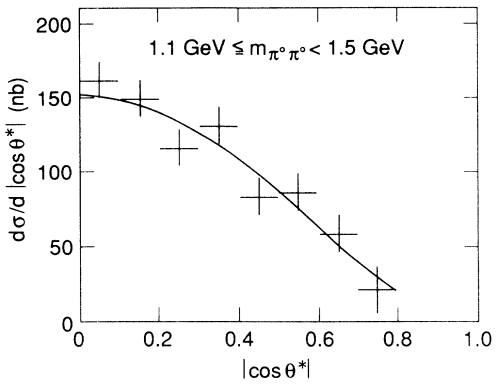

FIG. 10. Differential cross section $d\sigma/d|\cos\theta^*|$ in the $f_2(1270)$ region. Note that the fit yields pure $|Y_{22}|^2$ in this mass region.

This confirms the helicity-2 dominance for $f_2(1270)$ formation in quasireal two-photon collisions as expected from theory and as already observed by other experiments.

Using our upper limit on the spin-0 fraction in the $f_2(1270)$ region, we deduce the following 90%-C.L. upper limit:

$$\Gamma_{\gamma\gamma}(f_0(1300))B(f_0(1300)\to\pi^0\pi^0)<1.7 \text{ keV}$$

$$\text{for } \Gamma_{\text{tot}}(f_0(1300))<0.4 \text{ GeV} .$$

ACKNOWLEDGMENTS

We acknowledge useful discussions with T. Oest and J. Olsson. We would like to thank the DESY and SLAC directorates for their support. This experiment would not have been possible without the dedication of the DORIS machine group as well as the experimental support groups at DESY. The visiting groups thank the DESY laboratory for the hospitality extended to them. H. Marsiske acknowledges support from the Humbolt Foundation. Z.J., B. Muryn, B.N., and G.N. thank DESY for financial support. E.D.B., R.H., and K.S. have benefited from financial support from the Humboldt Foundation. K. Königsmann acknowledges support from the Heisenberg Foundation. This work was supported by Department of Energy Contracts Nos. DE-AC03-76SF00515, DE-AC03-81ER40050, DE-AC02-76ER03066, DE-AC02-76ER03064, DE-AC02-76ER03072, and DE-AC03-76SF00326, by National Science Foundation Grants Nos. PHY75-22980, PHY85-12145, PHY82-08761, and PHY81-07396, by Stichting voor Fundamenteel Onderzock der Matérie, Nederlandse Organisatie voor Zuiver-Wetenschappelijk Onderzock (FOM-ZWO, The Netherlands), by the German Bundesministerium für Forschung und Technologie Contracts Nos. 054 ER 11P(5), 054 HH 11P(7), and 054 WU 11P(1); and by the Deutsche Forschungsgemeinschaft.

TABLE VI. Limits on the spin-2, helicity-0 contribution to $f_2(1270)$ formation in two-photon collisions.

Helicity-0 fraction	Decay channel	Reference
<0.22 (90% C.L.)	$\pi^0\pi^0$	This experiment
$0.11\pm^{0\ 34}_{0\ 11}$	$\pi^0\pi^0$	Crystal Ball (Ref. 26)
<0.14 (90% C.L.)	$\pi^+\pi^-$	DELCO (Ref. 3)
<0.15 (95% C.L.)	$\pi^0\pi^0$	JADE (Ref. 24)
<0.15 (95% C.L.)	$\pi^+\pi^-$	Mark II (Ref. 29)

*Permanent address: DPHPE, Centre d'Etudes Nucléaires de Saclay, F-91191 Gif-sur-Yvette, France.

†Permanent address: Institute of Physics and Nuclear Techniques, AGH, PL-30055 Cracow, Poland.

[1]A. Courau *et al.*, Nucl. Phys. **B271**, 1 (1986); Z. Ajaltouni *et al.*, Phys. Lett. B **194**, 573 (1987); **197**, 565(E) (1987).

[2]Ch. Berger *et al.*, Z. Phys. C **26**, 199 (1984).

[3]R. P. Johnson, Ph.D. thesis, Stanford University, Report No. SLAC-REP-294, 1986 (unpublished).

[4]H. Aihara *et al.*, Phys. Rev. Lett. **57**, 404 (1986).

[5]M. Poppe, Int. J. Mod. Phys. A **1**, 545 (1986).

[6]R. L. Goble and J. L. Rosner, Phys. Rev. D **5**, 2345 (1972); R. L. Goble, R. Rosenfeld, and J. L. Rosner, *ibid.* **39**, 3264 (1989).

[7]G. Mennessier, Z. Phys. C **16**, 241 (1983); G. Mennessier and T. N. Truong, Phys. Lett. B **177**, 195 (1986).

[8]M. R. Pennington, in *Proceedings of the VIII International Workshop on Photon-Photon Collisions,* Shoresh, Jerusalem Hills, Israel, 1988, edited by U. Karshon (World Scientific, Singapore, 1988).

[9]K. M. Watson, Phys. Rev. **88**, 1163 (1952).

[10]H. Marsiske, Ph.D. thesis, Hamburg University, Report No. DESY F31-88-02, 1988.

[11]E. D. Bloom and C. W. Peck, Annu. Rev. Nucl. Part. Sci. **33**, 143 (1983); D. Antreasyan *et al.*, Phys. Rev. D **36**, 2633 (1987).

[12]D. A. Williams *et al.*, Phys. Rev. D **38**, 1365 (1988).

[13]D. Gelphman, Ph.D. thesis, Stanford University, Report No. SLAC-REP-286, 1985.

[14]However, a refined analysis of the full data sample taken with the Crystal Ball detector does show an indication of exclusive $\eta\eta$ production in two-photon collisions; see H. Marsiske and K. Wacker (unpublished).

[15]G. Bonneau, M. Gourdin, and F. Martin, Nucl. Phys. **B54**, 573 (1973).

[16]R. Ford and W. Nelson, Report No. SLAC-REP-210, 1978 (unpublished).

[17]Particle Data Group, G. P. Yost *et al.*, Phys. Lett. B **204**, 1 (1988).

[18]B. Muryn, in *Proceedings of the VIII International Workshop on Photon-Photon Collisions* (Ref. 8).

[19]T. E. Barnes, K. Dooley, and N. Isgur, Phys. Lett. B **183**, 210 (1987).

[20]M. R. Pennington (private communication).

[21]H. Pilkuhn, in *Landolt-Börnstein,* New Series, Vol. 6 (Springer, Berlin/Heidelberg/New York, 1972).

[22]J. M. Blatt and V. Weisskopf, *Theoretical Nuclear Physics* (Wiley, New York, 1952).

[23]All fits used a χ^2 method and have been performed with the fitting program MINUIT; see F. James and M. Roos, CERN

Program Library, long writeup D506. The errors quoted are MINOS errors.

[24]J. Olsson, in *Proceedings of the VIII International Workshop on Photon-Photon Collisions* (Ref. 8).

[25]H. Kolanoski, *Two-Photon Physics at e^+e^- Storage Rings,* (Springer Tracts in Modern Physics, Vol. 105) (Springer, Berlin, 1984); S. Cooper, Annu. Rev. Nucl. Part. Phys. **38**, 705 (1988).

[26]C. Edwards *et al.,* Phys. Lett. **110B**, 82 (1982).

[27]G. Gidal, in *Proceedings of the VIII International Workshop on Photon-Photon Collisions* (Ref. 8).

[28]The upper limit has been calculated taking into account the systematic error.

[29]J. H. Boyer, in *Proceedings of the VIII International Workshop on Photon-Photon Collisions* (Ref. 8); and Ph.D. thesis, University of California at Berkeley, Report No. LBL-27180, 1989.

[30]D. Antreasyan *et al.,* Phys. Rev. D **33**, 1847 (1986).

[31]S. B. Berger and B. T. Feld, Phys. Rev. D **8**, 3875 (1973).

[32]J. Babcoc and J. L. Rosner, Phys. Rev. D **14**, 1286 (1976).

[33]V. M. Budnev and A. E. Kaloshin, Phys. Lett. **86B**, 351 (1979).

[34]T. Barnes, in *Proceedings of the VII International Workshop on Photon-Photon Collisions,* Paris, France, 1986, edited by A. Courau and P. Kessler (World Scientific, Singapore, 1986).

[35]C. A. Dominguez and N. Paver, Z. Phys. C **39**, 39 (1988).

[36]N. N. Achasov, S. A. Devyanin, and G. N. Shestakov, Z. Phys. C **16**, 55 (1982).

[37]J. Weinstein and N. Isgur, Phys. Rev. D **27**, 588 (1983).

[38]L. D. Landau, Sov. Phys. Dokl. **60**, 207 (1948); C. N. Yang, Phys. Rev. **77**, 242 (1950).

[39]B. Schrempp-Otto, F. Schrempp, and T. F. Walsh, Phys. Lett. **36B**, 463 (1971); P. Grassberger and R. Kögerler, Nucl. Phys. **B106**, 451 (1976); H. Krasemann and J. A. M. Vermaseren, *ibid.* **B184**, 269 (1981).

[40]R. Brandelik *et al.,* Z. Phys. C **10**, 117 (1981).

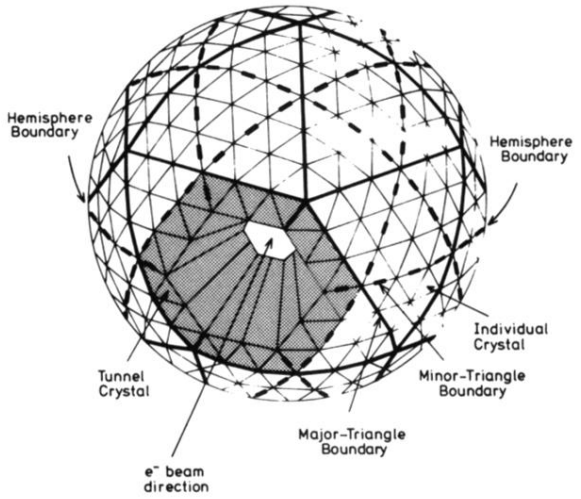

FIG. 1. Organization of the individual crystals into major and minor triangles, and into top and bottom hemispheres. The shaded area shows one group of tunnel crystals.